*Progress In Electromagnetics Research Letters, Vol. 49, 1–8, 2014*

# Dual-Band Bandpass Filter with Independently Tunable Passbands and Wide Stopband

**Yingfang Guo, Feng Wei*, Mingzhong Lin, and Xiaowei Shi**

**Abstract**—This paper presents a dual-mode stub loaded ring resonator (SLRR) to design a tunable dual-band bandpass filter (BPF) with two independently controllable passbands. The proposed resonator principally comprises a stepped-impedance ring resonator (SIRR) loaded with three stubs and two varactor diodes. Two independently tunable passbands are implemented by employing two varactors to control the dominant even-mode resonant frequency and odd-mode resonant frequency, respectively. Moreover, a new stub loaded double-ring resonator (SLDRR) is proposed to design the second tunable dual-band filter by shorting two stubs of the SLRR. With the same tuning method, the second filter can achieve two independently controllable passbands. In order to suppress the harmonics, defected ground structures (DGSs) are introduced at input and output feeding lines without degrading the passbands characteristics. The measured results are in good agreement with the simulated ones.

## 1. INTRODUCTION

As one of the essential components for the multiband and wireless communication systems, electrically tunable multiband bandpass filters (BPFs) have developed rapidly due to their potential for reducing system size, complexity and the cost in fabrication in recent years. Therefore, aggressive investment has been done based on different kinds of tuning devices. Recently, the tunable filters based on varactor diodes have been gaining much attention.

In [1], a dual-band filter is presented with only one passband can be tuned. A compact tunable dual-band filter is proposed in [2]. However, its two passbands can not be tuned independently since the odd- and even-mode are affected each other. A tunable dual-band filter is designed based on two single band filters using common input/output ports in [3], which is large in circuit size. Then, with the increasing demands for high signal quality and strong interference immunity, a broad stopband of the tunable filters is extremely desired. Some attempts have been made to solve this problem [4, 5]. In [4], multiple transmission zeros are generated to obtain harmonic suppression. However, this method can only suppress the harmonics around a specific frequency. Defected ground structures (DGSs) are regarded as a lowpass filter to remove spurious responses and obtain wide stopband characteristics in [5].

In this paper, a tunable dual-band BPF based on stub loaded ring resonators (SLRRs) is presented. Since the resonator is symmetrical, the odd- and even-mode method can be implemented. It is found that the two passbands depend on the even- and odd-mode capacitances and loaded stubs, respectively. Therefore, the proposed filter can achieve two independently controllable passbands. By shorting one end of the SLRR, a new stub loaded double-ring resonator (SLDRR) is obtained. With the same tuning method, an improved BPF with two separately tunable passbands is designed. Simultaneously, defected ground structures (DGSs) are introduced in this filter at input/output feeding lines to suppress the harmonics. The measured results are in good agreement with the simulated ones.

*Received 26 June 2014, Accepted 5 August 2014, Scheduled 7 September 2014*

* Corresponding author: Feng Wei (fwei@mail.xidian.edu.cn).

The authors are with the National Laboratory of Science and Technology on Antennas and Microwaves, Xidian University, Xi'an 710071, P. R. China.

## 2. THEORETICAL ANALYSIS

The basic structure of the proposed SLRR is demonstrated in Figure 1(a), where $Y_1$, $Y_2$ and $L_1$, $L_{1a}$, $L_{1b}$, $L_2$ denote the characteristic admittance and physical length, respectively. As shown, one varactor $C_{even}$ is placed at the end of the central stub, located in the symmetry plane with characteristic admittance of $Y_4$ and physical length of $L_4$. And the varactor $C_{odd}$ is attached between two stubs whose characteristic admittance is $Y_3$ and physical length is $L_3$. Synchronously, at the ends of the two stubs stand two identical capacitances of $C_1$. Since the structure is symmetrical, the even- and odd-mode analysis method can be applied to analyze the performance of the resonator. Therefore, a reference port is added for deriving an input admittance. To facilitate the analysis below, the parasitic effects of the varactors and line discontinuity are ignored.

### 2.1. Even- and Odd-mode Excitation Analysis

When the even-mode excitation is applied to proposed resonator shown in Figure 1(a), there is the perfect magnetic wall or ideal open-circuited terminal in equivalence along the symmetry plane. So the whole resonator can be represented by the half circuit, as given in Figure 1(b). The even-mode input admittance is determined as

$$Y_{ine} = jY_2 \frac{(Y_1Y_2\tan(\beta_e L_2) + Y_1^2\tan(\beta_e L_{1b})) + Y_{L\_even}(Y_1 - Y_2\tan(\beta_e L_{1b})\tan(\beta_e L_2))}{(Y_1Y_2 - Y_1^2\tan(\beta_e L_{1b})\tan(\beta_e L_2)) - Y_{L\_even}(Y_1\tan(\beta_e L_2) + Y_2\tan(\beta_e L_{1b}))} \tag{1}$$

with

$$Y_{L\_even} = Y_3\frac{\omega_e C_1 + Y_3\tan(\beta_e L_3)}{Y_3 - \omega_e C_1\tan(\beta_e L_3)} + Y_{L\_e\_1}$$

$$Y_{L\_e\_1} = Y_1\frac{Y_1\sin\beta_e(L_1+L_{1a}) + Y_4\dfrac{\omega_e C_{even} + 4Y_4\tan(\beta_e L_4)}{2Y_4 - \omega_e C_{even}/2\tan(\beta_e L_4)}\cos\beta_e(L_1+L_{1a})}{Y_1\cos\beta_e(L_1+L_{1a}) - Y_4\dfrac{\omega_e C_{even} + 4Y_4\tan(\beta_e L_4)}{2Y_4 - \omega_e C_{even}/2\tan(\beta_e L_4)}\sin\beta_e(L_1+L_{1a})}$$

where $\beta_e$ represents the phase constant at the even-mode resonant angular frequency $\omega_e$. The even-mode resonant frequencies can be found from (2).

$$\mathrm{Im}[Y_{ine}] = 0 \tag{2}$$

The fundamental even-mode resonant frequency can be utilized to implement the first passband frequency. Substituting (1) into (2), it is found that the even-mode resonant frequency depends on $C_1$ and $C_{even}$. Meanwhile it is mostly affected by the central loaded stub $L_4$, although the two open stubs

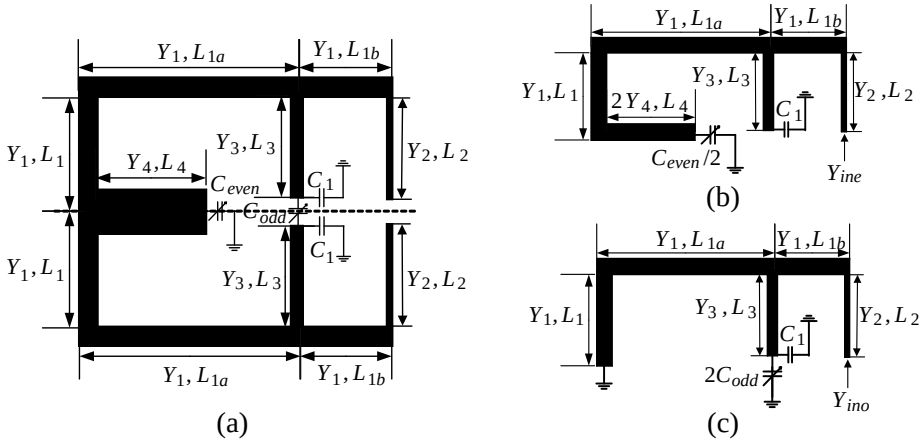


**Figure 1.** (a) Schematic of the proposed SLRR. (b) Equivalent even-mode circuit. (c) Equivalent odd-mode circuit.

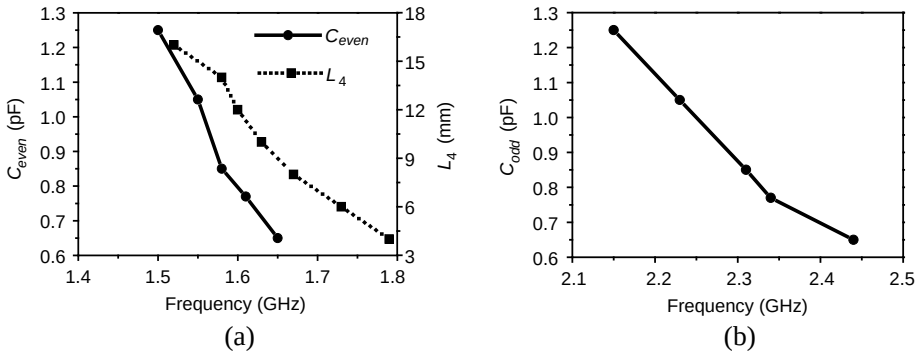


**Figure 2.** The variation of the even- or odd-mode resonant frequencies. (a) The even-mode frequency versus $C_{even}$ and $L_4$. (b) The odd-mode frequency versus $C_{odd}$.

work in it as well. Thus, changing $C_1$ or $C_{even}$ will result in the variation of the resonant frequency, enabling the tuning of the first passband frequency. Moreover, when $C_1$ is fixed, the even-mode resonant frequency can be tuned by $C_{even}$ absolutely.

Figure 2(a) shows the variation of the even-mode resonant frequency versus $C_{even}$ and $L_4$. By varying $C_{even}$ from 0.65 to 1.25 pF, the even-mode resonant frequency can be changed from 1.5 to 1.65 GHz. When $L_4$ increases from 4 to 16 mm, the even-mode resonant frequency decreases from 1.8 to 1.5 GHz. Selecting appropriate $L_4$, the characteristic discussed above makes it possible to design a dual-band BPF with controllable first passband and fixed second passband.

Similarly, the odd-mode resonant frequency can be acquired. And the fundamental odd-mode resonant frequency can be adopted to constitute the second passband frequency. It is learned that the odd-mode resonant frequency varies with $C_1$ and $C_{odd}$. Simultaneously it is influenced by the two stubs. Hence when $C_1$ is fixed, the odd-mode resonant frequency is completely controlled by $C_{odd}$. Figure 2(b) reveals the variation of the odd-mode resonant frequency versus $C_{odd}$. By varying $C_{odd}$ from 0.65 to 1.25 pF, the odd-mode resonant frequency reduces from 2.45 to 2.15 GHz. This property can be used to design a dual-band BPF with a fixed first passband and controllable second passband.

In conclusion, fixing $C_1$, $C_{even}$ affects only the even-mode resonant frequencies and does not matter the odd-mode ones. While $C_{odd}$ only has an effect on the odd-mode resonant frequencies and does not concern the even-mode ones. Irrelevant to the resonant frequencies of odd mode, the central loaded stub merely has an influence upon the resonant frequencies of even mode. Whereas the two open stubs react on both even- and odd-mode resonant frequencies, but mainly on even mode. Consequently, a dual-band BPF with independently controllable dual passbands becomes realizable.

### 2.2. Coupling Coefficient

To determine the bandwidth of a filter, the coupling coefficient $K_i$ and the external quality factor $Q_e$ should be studied. For the proposed two-order filter, the coupling coefficient $K_1$ of the first passband, corresponding to the even mode, can be calculated by the following formula

$$K_1 = \frac{f_{e2}^2 - f_{e1}^2}{f_{e2}^2 + f_{e1}^2} \tag{3}$$

Similarly, for the odd-mode case, the coupling coefficient $K_2$ of the second passband can be obtained. Figure 3(a) plots the calculated coupling coefficients for the first and second passbands under different $S$, which is the gap width of the coupling line. It can be seen that the coupling coefficients $K_1$ and $K_2$ decrease as $S$ increases. By choosing the appropriate value of $S$, a required bandwidth can be obtained.

### 2.3. External Quality Factor

Another factor affecting the bandwidth is the external quality factor $Q_e$. With the $I/O$ coupling, the circuit models for the even and odd modes are present in Figures 4(a) and (b), respectively. Seen

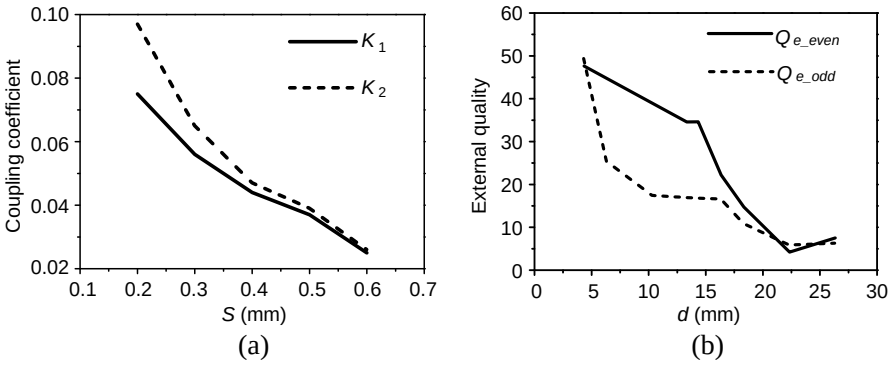


**Figure 3.** The variation of the coupling coefficients and external quality factors for the first and second passbands. (a) The coupling coefficients versus $S$. (b) The external quality factors versus $d$.

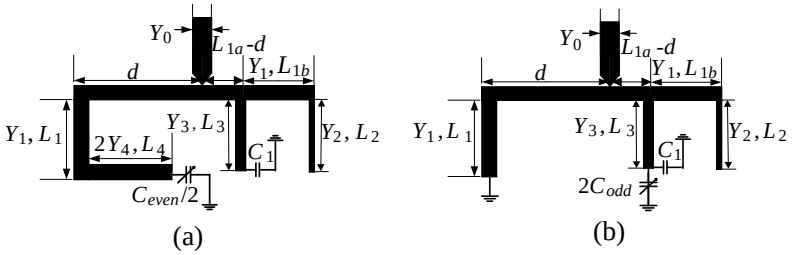


**Figure 4.** Equivalent circuits with distinct $I/O$ couplings. (a) Even-mode case. (b) Odd-mode case.

from the input port whose position is characterized by the tap position d, the whole even- mode input admittance $Y_{i/o\_ine}$ is

$$Y_{i/o\_ine} = jY_1\left(\frac{Y_1\tan(\beta_e(L_{1a}-d))+\mathrm{Im}[Y_{ine\_2}]}{Y_1-\mathrm{Im}[Y_{ine\_2}]\tan(\beta_e(L_{1a}-d))}+Y_{ine\_1}\right) \tag{4}$$

where

$$\begin{aligned}
Y_{ine_1} &= \frac{Y_1\tan(\beta_e(L_{1a}-d))+Y_4\dfrac{\omega_e C_{even}+4Y_4\tan(\beta_e L_4)}{2Y_4-\omega_e C_{even}/2\tan(\beta_e L_4)}}{Y_1-Y_4\dfrac{\omega_e C_{even}+4Y_4\tan(\beta_e L_4)}{2Y_4-\omega_e C_{even}/2\tan(\beta_e L_4)}\tan(\beta_e(L_{1a}-d))}\\
Y_{ine_2} &= jY_2\frac{(Y_1Y_2\tan(\beta_e L_2)+Y_1^2\tan(\beta_e L_{1b}))+Y_{ine_3}(Y_1-Y_2\tan(\beta_e L_{1b})\tan(\beta_e L_2))}{(Y_1Y_2-Y_1^2\tan(\beta_e L_{1b})\tan(\beta_e L_2))-Y_{ine_3}(Y_1\tan(\beta_e L_2)+Y_2\tan(\beta_e L_{1b}))}\\
Y_{ine_3} &= Y_3\frac{\omega_e C_1+Y_3\tan(\beta_e L_3)}{Y_3-\omega_e C_1\tan(\beta_e L_3)} \quad \beta_e=\frac{\omega_e}{\upsilon_p}
\end{aligned}$$

Then the external quality factor $Q_{e\_even}$ for even mode is determined as

$$Q_{e\_even} = \frac{\omega_0}{2Y_0}\frac{\partial \mathrm{Im}[Y_{i/o\_ine}]}{\partial\omega_e}\bigg|_{\omega_e=\omega_0} \tag{5}$$

Similarly, for the odd mode case, the external quality factor $Q_{e\_odd}$ can be obtained as

$$Q_{e\_odd} = \frac{\omega_0}{2Y_0}\frac{\partial \mathrm{Im}[Y_{i/o\_ino}]}{\partial\omega_o}\bigg|_{\omega_o=\omega_0} \tag{6}$$

Figure 3(b) plots the external quality factors $Q_{e\_even}$ and $Q_{e\_odd}$, corresponding to the first and second passbands respectively, under different $d$. It can be seen that increasing $d$ leads to the decrease of $Q_{e\_even}$ and $Q_{e\_odd}$ in general. Therefore, by properly choosing the parameter $d$, the desired quality factors can be obtained within the frequency tuning range.

## 3. FILTER IMPLEMENTATION AND VERIFICATION

Based on the previous design theory, two tunable dual-band BPFs are implemented. The used substrate is Teflon with a dielectric constant of 2.65 and thickness of 0.8 mm. The proposed filters employ the varactor diodes with two types of packaging from the Skyworks: SMV1405-079LF for tuning $C_{even}$ and SMV1405-074LF for tuning $C_{odd}$, respectively.

### 3.1. Filter I: Tunable Dual-Band BPF without Harmonic Suppression

Figure 5 shows the schematic layout of the proposed first tunable dual-band BPF (filter I). It is composed of two SLRRs. The input and output feed lines are located symmetrically at the center, resulting in a transmission zero between the two passbands. Meanwhile they are tapped at the resonators. And the tap position d is tuned to fulfill the requirement of the filter over the frequency tuning range. In addition, two short transmission lines with characteristic admittance of $Y_5$, physical length of $L_5$ and distance of $g$, lie to the coupling parts of the two resonators to improve the filter performance [6]. Table 1 lists the specific parameters for the proposed filter I measured with a vector network analyzer (Agilent N5230A).

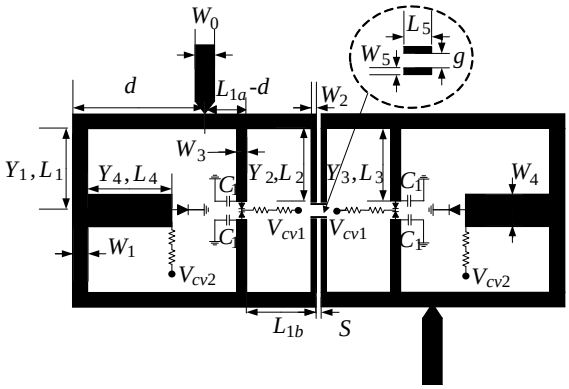


**Figure 5.** Schematic of the proposed first tunable dual-band BPF.

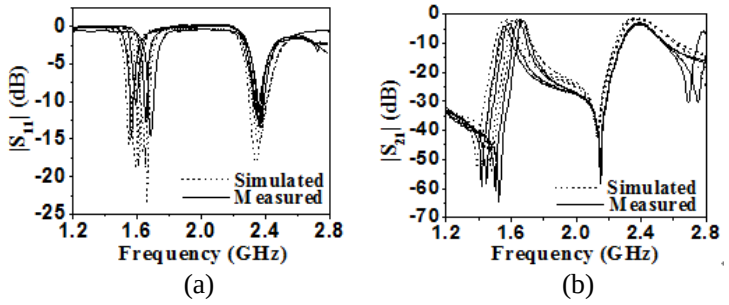


**Figure 6.** Simulated and measured results of the tunable dual-band filter I with the fixed second passband and tunable first passband. (a) $S_{11}$-magnitude. (b) $S_{21}$-magnitude.

**Table 1.** Parameters of the proposed first tunable dual-band BPF (in millimeters).

| $L_1$ | $L_{1a}$ | $L_{1b}$ | $L_2$ | $L_3$ | $L_4$ | $L_5$ | $S$ | $g$ | $C_{odd}$ |
|---|---|---|---|---|---|---|---|---|---|
| 10.1 | 20.6 | 7.6 | 9 | 8.9 | 10 | 1.8 | 0.6 | 1.6 | 0.63∼1.17 pF |
| $W_0$ | $W_1$ | $W_2$ | $W_3$ | $W_4$ | $W_5$ | $d$ | $C_1$ | | $C_{even}$ |
| 2.2 | 1.8 | 0.6 | 1.2 | 4 | 0.15 | 14.3 | 0.2 pF | | 0.63∼1.17 pF |

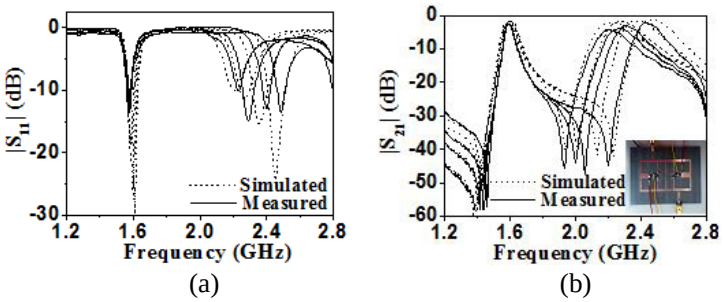


**Figure 7.** Simulated and measured results of the tunable dual-band filter I with the fixed first passband and tunable second passband. (a) $S_{11}$-magnitude. (b) $S_{21}$-magnitude.

Figures 6(a) and (b) show the simulated and measured results of the tunable dual-band filter I with the fixed second passband and tunable first passband in their center frequencies. The second-passband center frequency is fixed at 2.4 GHz, and the first-passband center frequency is tuned from 1.50 to 1.65 GHz with the approximate 3-dB fractional-bandwidth (FBW) of 1.3% and frequency tunability of 12.9%. Figures 7(a) and (b) demonstrate the simulated and measured results of the tunable filter I with the fixed first passband and tunable second passband. Fixing the first-passband center frequency at 1.55 GHz, the second-passband center frequency is tuned from 2.26 to 2.53 GHz with the almost 3-dB FBW of 4.3% and frequency tunability of 11.3%. It is found from the results that the return loss is better than 10 dB and the insertion loss less than 5 dB over the entire tuning range.

### 3.2. Filter II: Tunable Dual-Band BPF with Harmonic Suppression

From the simulated and measured results described in filter I, it is found that the filter performance can be improved due to two short transmission lines. Therefore, in the second tunable dual-band BPF (filter II), one end of the stub loaded ring resonator (SLRR) is short-circuited to achieve a better performance, and moreover, this action obtains a stub loaded double-ring resonator (SLDRR) and decreases the frequency of the filter. In filter I, the second harmonic of the first passband is quite close to the second passband. When the second passband is fixed and the first passband tuned, the harmonics will degrade the second passband. The first section introduces several methods to suppress harmonics and DGS is adopted in filter II. Non-uniform H-shaped DGS forms [7], using S-shaped gap replacing the general gap to reduce the frequency [8], are defected at the input/output feeding lines to induct

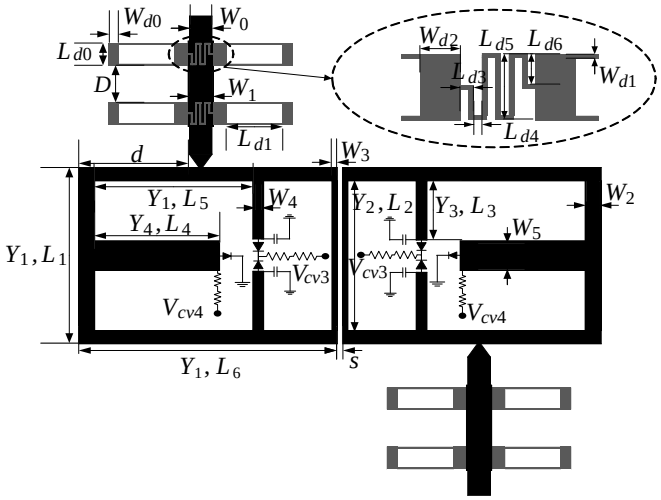


**Figure 8.** Schematic of the proposed second tunable dual-band BPF with harmonic suppression.

**Table 2.** Parameters of the second tunable dual-band BPF with harmonic suppression (in millimeters).

| $L_1$ | $L_2$ | $L_3$ | $L_4$ | $L_5$ | $L_6$ | $d$ | $S$ | $W_{d1}$ | $W_{d2}$ | $L_{d0}$ | $L_{d1}$ | $L_{d2}$ | $L_{d3}$ |
|---|---|---|---|---|---|---|---|---|---|---|---|---|---|
| 23.8 | 20.2 | 8.9 | 14 | 17.6 | 28.8 | 13.5 | 0.6 | 0.2 | 1.2 | 3 | 16.2 | 0.5 | 0.3 |
| $W_0$ | $W_1$ | $W_2$ | $W_3$ | $W_4$ | $W_5$ | $D$ | $W_{d0}$ | $L_{d4}$ | $L_{d5}$ | $C_1$ | $C_{even}$ | $C_{odd}$ | |
| 2.24 | 2.8 | 1.8 | 0.6 | 1.2 | 4 | 5 | 1.2 | 2.8 | 1.4 | 0.2 pF | 0.63∼2 pF | 0.77∼2.63 pF | |

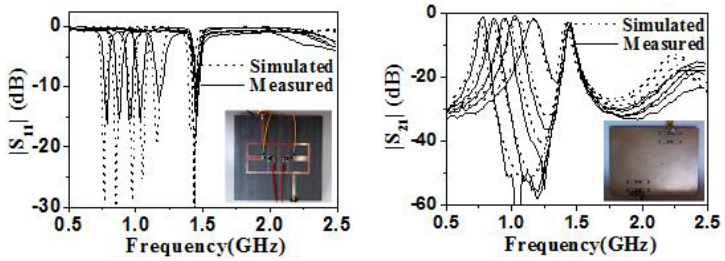


(a) (b)

**Figure 9.** Simulated and measured results of the improved tunable dual-band filter II with fixed second passband and tunable first passband. (a) $S_{11}$-magnitude. (b) $S_{21}$-magnitude.

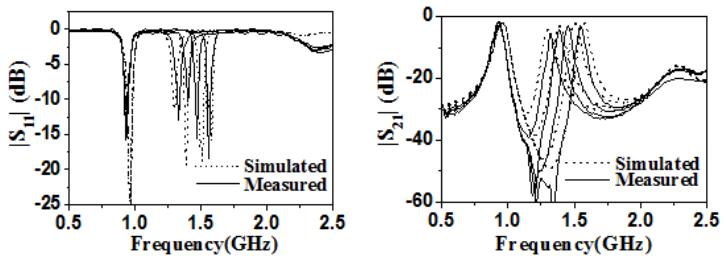


(a) (b)

**Figure 10.** Simulated and measured results of the improved tunable dual-band filter II with fixed first passband and tunable second passband. (a) $S_{11}$-magnitude. (b) $S_{21}$-magnitude.

coupling and reject band. Meanwhile, the application of compensated microstrip line, which forms a lowpass filter (LPF) with the DGSs, enhances the performance of the LPF [9]. Figure 8 illustrates the configuration of the proposed filter II, and Table 2 gives its parameters.

The simulation and measurement results of filter II are revealed in Figures 9 and 10. The passband frequencies are controlled with the help of the bias voltages of the varactor diodes. From Figures 9(a) and (b), it is observed of the tunable dual-band filter II with the fixed second passband and tunable first passband in their center frequencies.

The second passband is fixed at 1.45 GHz, and the first-passband frequency can be tuned from 0.78 to 1.18 GHz with the 3-dB FBW of 6.9%–8.5% and the frequency tunability of 40.82%. While as shown in Figures 10(a) and (b), the second passband frequency can be tuned from 1.37 to 1.63 GHz with the almost constant 3-dB FBW of 7.3% and the frequency tunability of 17.33%, when the first passband is fixed at 0.95 GHz. It is illustrated that the return loss is better than 10 dB and the insertion loss less than 4.5 dB over the tuning range. As demonstrated above, the performance of filter II is largely improved in comparison to filter I. The comparisons of the filter II with other reported dual-band filters in performance are summarized in Table 3. The proposed filter II can provide independent dual-passband characteristics and the first passband controlled by the varactor diodes between two stubs have a wider tuning range. Moreover, the second passband achieves almost constant bandwidth.

**Table 3.** Comparisons in performances of tunable dual-band filters.

| | Frequency Tunable [GHz] | | 3-dB Bandwidth Variation | | Insertion Loss [dB] | |
|---|---|---|---|---|---|---|
| | $f_1$ | $f_2$ | $f_1$ | $f_2$ | $f_1$ | $f_2$ |
| [1] | Fixed @ 2.43 | 5.28–5.74 | 13.58% | 5.9–8.6% | 1.8 | 2.3–4.5 |
| [2] | 1.48–1.80 | 2.40–2.88 | 5.7–8.5% | 8.2–12.4% | 1.99–4.4 | 1.6–4.2 |
| [3] | 2.20–2.70 | 3.45–4.20 | × | × | 3–5 | 4–6 |
| Filter II | 0.78–1.18 | 1.37–1.63 | 6.9–8.5% | About 7.3% | 1.4–2.6 | 2.2–4.5 |

Filter II = Filter II of this work; × = not mentioned in the paper.

## 4. CONCLUSION

In this paper, a stub loaded ring resonator (SLRR) with two independently tunable passbands has been designed. The proposed resonator can independently determine the odd- and even-mode resonant frequencies by different varactor diodes and stubs. To improve the performance, a stub loaded double-ring resonator (SLDRR) is presented and DGSs are employed to suppress harmonics. Both the theoretical analysis and experiments are provided to validate the proposed structures. The results show that the filters' passbands controlled by the varactor diodes have a wider tuning range. And the harmonics can be suppressed without degrading the passband performance. Due to their simple structure and good performance, the proposed filters are attractive for use in future reconfiguration systems.

## ACKNOWLEDGMENT

This work was supported by the National Natural Science Foundation of China (NFSC) under Grant 61301071 and China Scholarship Council.

## REFERENCES

1. Girbau, D., A. Lazaro, E. Martinez, D. Masone, and L. Pradell, "Tunable dual-band bandpass filter for WLAN applications," *Microw. Opt.Technol. Lett.*, Vol. 51, No. 9, 2025–2028, Sep. 2009.
2. Chaudhary, G., Y. Jeong, and J. Lim, "Harmonic suppressed dual-band bandpass filters with tunable passbands," *IEEE Trans. Microw. Theory Tech.*, Vol. 60, No. 7, 2115–2123, Jul. 2012.
3. Djoumessi, E. E., M. Chaker, and K. Wu, "Varactor-tuned quarter-wavelength dual-bandpass filter," *IET Microw. Antennas & Propag.*, Vol. 3, No. 1, 117–124, Feb. 2009.
4. Kuo, J. T. and H. P. Lin, "Dual-band bandpass filter with improved performances in extended upper rejection band," *IEEE Trans. Microw. Theory Tech.*, Vol. 57, No. 4, 824–829, Apr. 2009.
5. Boutejdar, A., A. Batmanov, A. Elsherbini, E. P. Burte, and A. S. Omar, "A new compact tunable bandpass filter using defected ground structure with active devices," *IEEE Antennas and Propagation Society International Symposium*, 1–4, 2008.
6. Wang, X. H., L. Zhang, Y. F. Bai, Y. Xu, H. Xu, and X. W. Shi, "Compact tunable dual-band filter using SIRs without extra blocking capacitances," *Journal of Electromagnetic Waves and Applications*, Vol. 27, No. 5, 544–551, 2013.
7. Boutejdar, A., A. Elsherbini, and A. Omar, "Design of a novel ultra-wide stopband lowpass filters using H-defected ground structure," *Microw. Opt. Technol. Lett.*, Vol. 50, No. 3, 771–775, 2008.
8. Park, J. S., J. S. Yun, and C. S. Park, "DGS resonator with interdigital capacitor and application to bandpass fiter design," *Electron. Lett.*, Vol. 40, No. 7, 433–434, 2004.
9. Lim, J. S., C. S. Kim, Y. T. Lee, D. Ahn, and S. Nam, "Design of lowpass filters using defected ground structure and compensated microstrip line," *Electron. Lett.*, Vol. 38, No. 22, 1357–1358, 2002.